Impact of Monsoon Rainfall on Roadside Slopes

Laxmi Adhikari[1], Jayant Bhatt[1], Shreejan Bikram Thapa[1], Lipika Maharjan[1], Kushal Dahal[1], Madan Rimal[1], Prajwal Timilsina[1] Bhim Kumar Dahal[1]*
[1]Department of Civil Engineering, Institute of Engineering, Pulchowk Campus, Tribhuvan University, Nepal
*Corresponding Author: bhimd@pcampus.edu.np

Abstract

Monsoon-induced landslides pose a severe threat to Nepal's hilly and mountainous regions, frequently causing highway disruptions and substantial loss of life and property every year. This study examines a 4 km section of the Dakshinkali-Kulekhani road to assess the effects of monsoon rainfall on roadside slope stability. Field data, including slope geometry, land use, and the presence and condition of erosion control measures (ECM), were recorded before and after the monsoon, alongside photographic documentation at each chainage of the study route. Rainfall data were collected for the study area, and soil samples from failed sections underwent laboratory tests to determine relevant index and engineering properties. Slope stability analysis combined with transient seepage modeling was performed using GeoStudio on key sections with slope failures. Among 188 sections under considerations, 62 experienced significant slope failures, predominantly in areas lacking effective ECM; even where ECM existed, they were often insufficient and showed considerable collapse post-monsoon. Most of the failures occurred on slopes excavated on soft rocks. A strong inverse relationship was observed between rainfall intensity and factor of safety, with four critical high-rainfall days causing rapid declines in factor of safety through rainwater infiltration. This study underscores the urgent need for improved and site-specific slope protection strategies to mitigate landslide risks under intense monsoon conditions in Nepal's mountainous terrain.

Keywords: Erosion Control Measures, Monsoon rainfall, Slope stability, Volumetric Water Content,

Introduction

Nepal is located in a tectonically active region dominated by the young Himalayan Range, characterized by rugged topography, unstable geological structures, and soft, fragile rocks (Dahal & Hasegawa, 2008). The country experiences intense monsoon rainfall from June to September, which accounts for about 80% of its annual precipitation (Karki et al., 2017). In extreme instances, up to 10% of the yearly precipitation can fall in a single day, and often 50% may occur within just 10 days during the monsoon (Dahal & Hasegawa 2008). This concentrated rainfall pattern plays a significant role in triggering slope failures by rapidly saturating soil, increasing pore water pressure, promoting erosion, reactivating dormant landslides, and causing toe erosion (Liu et al. 2021). Recent studies have confirmed a strong link between monsoon rainfall intensity and fatal landslides in Nepal (Petley et al., 2007; Sitaula et al., 2023). Globally, rainfall-induced landslides cause substantial economic losses every year, with Nepal ranking as the third most affected country (Sim et al., 2022). Slope failures induced by rainfall arise when infiltrating water raises pore water pressure, reducing soil shear strength by decreasing cohesion and internal friction (Iverson, 2000; Fredlund & Rahardjo, 1993). In Nepal's steep mountainous terrain, landslides frequently occur along road corridors, especially where slopes have been modified for road construction without proper design, mitigation measures, or vegetation cover, and where spoil disposal is poorly managed (Dahal et al., 2006; McAdoo et al., 2018). Seasonal wetting and drying cycles further degrade slope stability over time (Gunn et al., 2018). Additionally, seismic activity in the Nepal Himalaya exacerbates slope instability, particularly in slopes already weakened by intense monsoon rainfall (Pyakurel et al., 2024).

These combined factors cause significant damage every monsoon season to infrastructure, human lives, and livelihoods. In 2024 alone (up to October 3), monsoon-related floods and landslides caused at least 236 deaths, 19 missing persons, and 165 injuries. The Department of Roads (DOR) preliminarily estimated NPR 2.52 billion in damages to roads and bridges - NPR 1.50 billion for roads and NPR 1.02 billion for bridges. The disasters affected 44 bridges and disrupted transportation on 24 sections of 10 major highways. Including impacts on irrigation, hydropower, agriculture, and telecommunications, the total economic loss exceeds NPR 13.4 billion, along with thousands of affected households (Ministry of Home Affairs, 2024).

Laxmi Adhikari et. al.

Addressing these severe challenges requires a comprehensive understanding of how monsoon rainfall impacts roadside slope stability and a critical evaluation of current erosion and drainage control methods to foster sustainable slope stabilization for hill road networks (Paudyal et al. 2023). This research focuses on the Dakshinkali–Kulekhani road section in Kathmandu District, Bagmati Province, assessing monsoon rainfall effects on slope stability through pre- and post-monsoon field surveys, laboratory tests, and slope stability modeling. The study quantifies rainfall-induced slope behavior changes and proposes suitable ECM intending to help develop more durable and climate-resilient slope protection systems for mountainous roads in Nepal.

Study Area

The study was conducted along a 4.031 km section of the Dakshinkali-Kulekhani road, located in Kathmandu District, Bagmati Province, Nepal (Figure 1). The road section extends from 27°36′05″ N, 85°15′55″ E at its starting point to 27°35′02″ N, 85°15′19″ E at its end point. Elevation along the profile ranges from a minimum of 1502 m to a maximum of 1649.52 m above mean sea level, with an average elevation of approximately 1572.6 m.
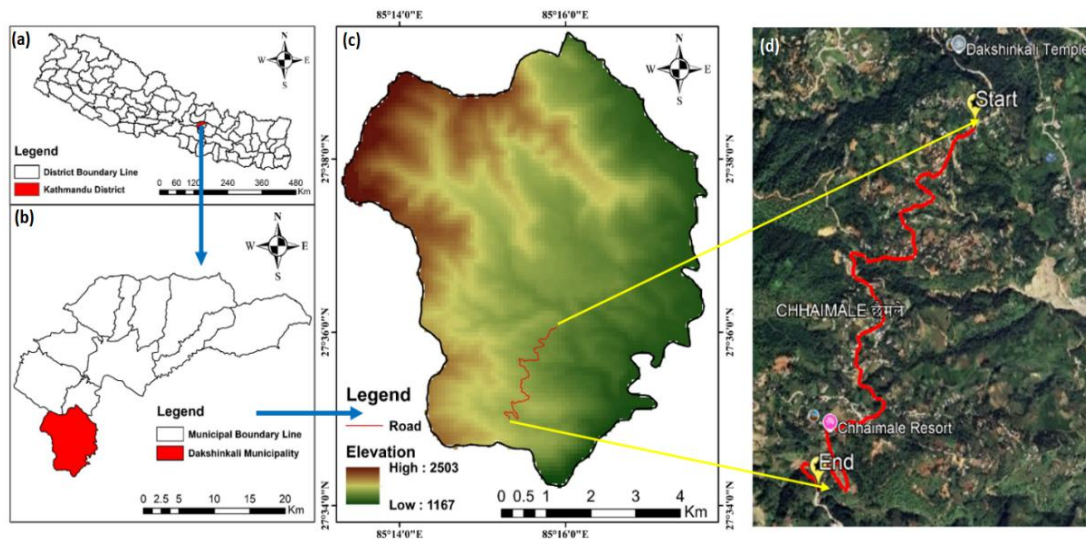

Figure 1: Study Area; (a) Map of Nepal showing Kathmandu District, (b) Map of Kathmandu District divided into municipalities and showing Dakshinkali Municipality, (c) Elevation map of Dakshinkali Municipality including road alignment, and (d) Satellite Map of the alignment part
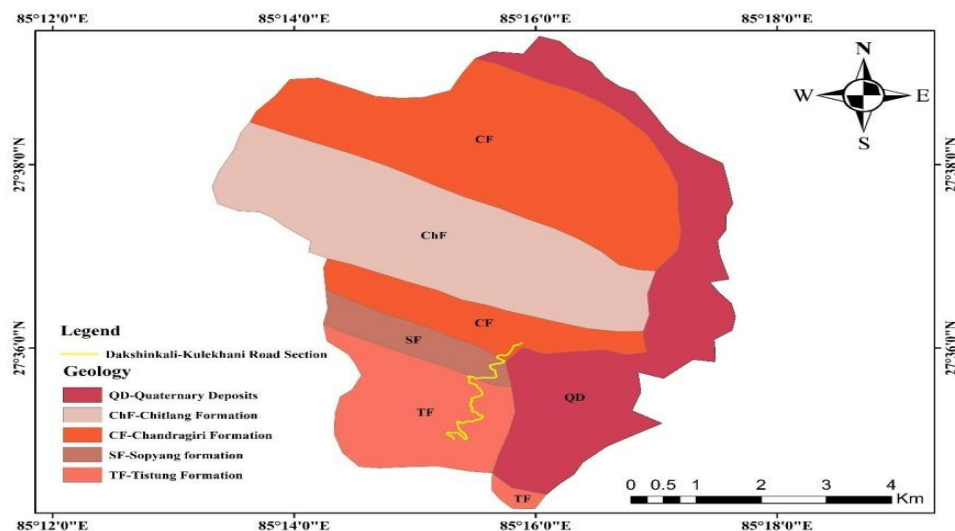

Figure 2: Regional geology of the study area

Geologically, the majority of the studied road section lies within the Lesser Himalaya Zone, with the Tistung Formation as presented in Figure 2. The governing rock types in the formations are phyllite and metasandstone.

Methodology

The general methodology of the research work is as shown in Figure 3. After the desk study and the review of available literature, reports, geological map, topographical map and the hydrological data, and considering the proximity and the newly constructed road section, the study site was selected. Since the objective was to evaluate the effect of monsoon rainfall on roadside slopes, the field assessment prior to monsoon was conducted throughout the 4 km road section, documenting the slope geometry, slope aspect, land use, and the present condition, and appropriate dimensional measurements of existing mitigation measures in the study area. In addition to these measurements, photographs were taken at each chainage to document the baseline site conditions before the monsoon season.
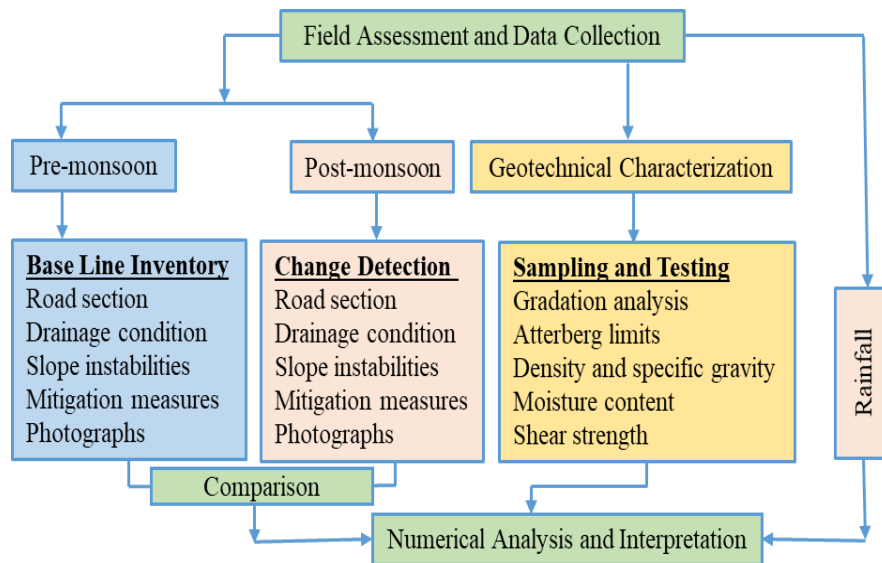

Figure 3: Flowchart showing methodology

The post-monsoon field assessment was conducted after the end of the monsoon season, focusing on sections with significant changes in the slope geometry and the performance of mitigation measures in controlling slope failures. Soil Samples, both disturbed and undisturbed, were collected for laboratory testing from the chainages that experienced severe slope failures. Using the field data and photographs, a comparative analysis was carried out, and the numerical analysis was performed using GeoStudio software to establish the effect of monsoon rainfall on the factor of safety of roadside slopes in the Lesser Himalaya. The key features are further elaborated hereunder.

Laboratory Tests

Engineering properties of the collected soil samples were tested in the Central Material Testing Laboratory, Institute of Engineering, Pulchowk Campus. The tests performed were particle size distribution, consistency limits and shear strength tests.

Numerical Analysis

The sections were defined in 2D geometry, using slope geometry data from field measurements, in CAD software, and then imported into the stability analysis software. Since the subsurface conditions were unknown due to the limitations of the survey, bedrock depth was assumed according to the site's proximity to surface water bodies, following the natural hill slope. The piezometric surface was introduced a few meters above the bedrock.
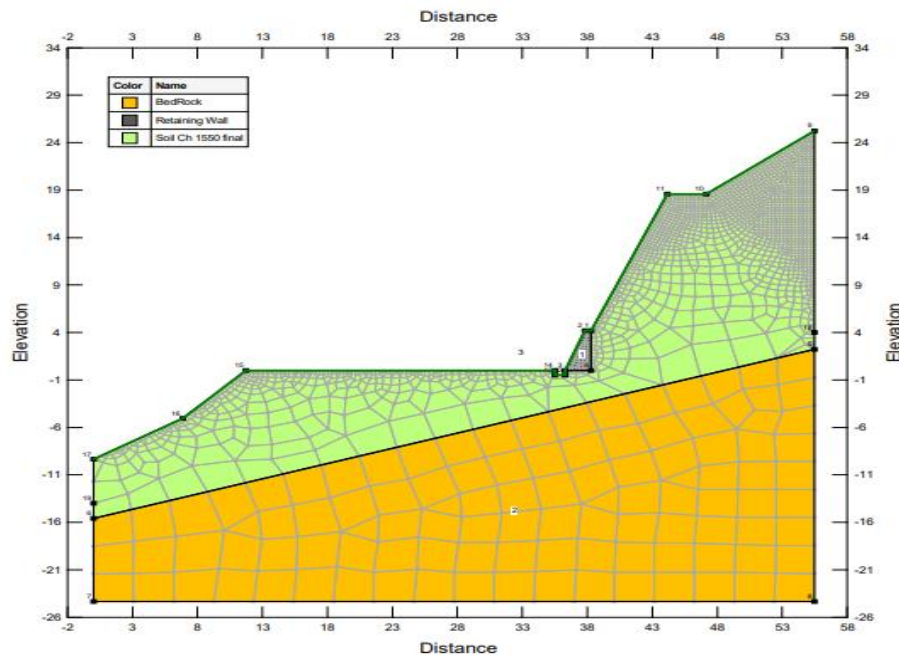
Figure 4: Model showing geometry and meshing

The general model and meshing is illustrated in Figure 4. The element sizes were reduced by a factor of 10 at the surface for a finer mesh. For the slope stability analysis, the Morgenstein-Price method with a half-sine interslice function was used. Similarly, the entry and exit for the slip surfaces were searched within a fixed range with 16 increments over the range and 8 radius increments. Porewater pressure condition was imported from the transient seepage analysis to simulate the effect of rainfall. The initial condition was defined from the drawn piezometric surface. These preferences were kept the same throughout all the sections under analysis for consistency.

Materials Model

The slope stability material properties of the soil, retaining wall, and gabion wall were defined using the Mohr-Coulomb material model (GEOSLOPE, 2022), while the Hoek-Brown material model (GeoSlope, 2022) was implemented for bedrock. Suction was considered for soil only, using the Volumetric Water Content (VWC) function estimated from grain size data (Van Genuchten, 1991; Schneider et al., 2012). For the Hydraulic material model, soil was considered for both saturated and unsaturated models, deriving the hydraulic conductivity function from Van-Genuchten estimation and the existing VWC function (Table 1).

Table 1: Soil suction parameters

Soil type	Residual water content	Saturated water content (w_{sat})	Residual water content (% of w_{sat})	Saturated Conductivity (mm/hr)
Sandy loam	0.065	0.41	15.853	12
Loamy sand	0.057	0.41	13.902	12

Results and discussion

Material Properties

Soil

The collected samples were tested in the laboratory, and the results are presented in the **Error! Reference source not found.**. Based on the textural classification, the soil samples from different

failure sites can be classified as loamy sand or as sandy loam, with the majority of the soil having silt particles with minimal cohesion, while the friction angle was more than 30 degrees.

Table 2: Laboratory results

Chainage	Descriptions	Unit weight (kN/m²)	c (kN/m²)	ø (°)	D10	D60	LL (%)
0+640	Loamy Sand	18.18	0	36.22	0.048	0.072	30.80
0+740	Sandy Loam	14.70	3.25	31.49	0.037	0.066	32.90
0+980	Loamy Sand	18.18	0	32.38	0.051	0.071	27.57
1+550	Sandy Loam	14.70	4.44	34.70	0.033	0.068	43.97
1+760	Sandy Loam	18.11	5.60	34.31	0.042	0.068	28.06
3+987	Loamy Sand	18.96	0	31.53	0.050	0.070	23.77

Rock

The properties of the bedrock were taken from different literature sources (Hoekt & Brown, 1997) and the field observation. The selected parameters for the analysis are presented in Table 3.

Table 3: Material properties for bedrock

Parameters	Unit weight (γ) (kN/m³)	Material constant of intact rock (m_i)	Geological Strength Index (GSI)	Disturbance factor (D)
Values	22	10	38	0

Confining stress (σ_3) (kN/m²)	Uniaxial Compressive Strength (UCS) (kN/m²)	Saturated conductivity (k_{sat}) (mm/hr)	Saturated Volumetric Water Content, VWC
250	50000	0.036	0.00897

Retaining wall

Properties of the retaining wall, i.e. cement stone masonry and gabion wall, are presented in **Error! Reference source not found.**. The properties considered for the modelling were carefully selected after analysis from the different literature (Schneider et al., 2012; Alias et al., 2020; Voit & Kuschel, 2020; Ayyub et al., 2021).

Table 4: Material properties for retaining wall

Materials	c (kN/m²)	ø (°)	γ (kN/ m³)	k_{sat} (m/sec)	Saturated VWC
Cement stone masonry	500	45	24	5.67×10^{-13}	0.136
Gabion	100	40	20	347.22	0.22

Back analysis

In the preliminary analyses, the soil strength parameters (c and ø) were obtained from laboratory test results (**Error! Reference source not found.**). These parameters were initially applied to a homogeneous soil profile in the model, which did not fully capture the actual site conditions, as soil properties can vary with depth. To more accurately represent the subsurface variability, the values of c and ø were later adjusted using field observations, engineering judgment, and back analysis (**Error!**

Reference source not found.). This modification resulted in a more realistic depiction of ground conditions and enhanced the reliability of the analysis.

Table 5: Modified data for back analysis

Chainage	0+980	1+760	Chainage	0+980	1+760
Cohesion (c) (kN/m^2)	2 kPa	7.1 kPa	cohesion (c) (kN/m^2)	2 kPa	7.1 kPa
ø (°)	39	38	ø (°)	39	38

Monsoon rainfall

Rainfall data were collected from the Department of Hydrology and Meteorology (DHM), Nepal, for the nearest meteorological station, focusing on hourly and daily rainfall intensities during the monsoon season.

Roadside failure during monsoon

The field observations clearly demonstrated the significant impact of monsoon rainfall on slope stability. Within a relatively short 300 m stretch of the road from chainage 1+450 m to 1+778 m, three uphill slopes and one downhill slope exhibited notable failures as depicted in Figure 5. For example, at chainage 1+450 m (uphill), a shallow-seated planar failure with a crown height of approximately 4.8 m occurred, causing accumulation of landslide debris that blocked side drains and obstructed surface drainage. Similarly, at chainage 1+550 m (uphill), erosion and sliding with a crown height of 8 m were observed, intensified by pre-existing gullies and steep slopes; this erosion extended about 40 m along the road corridor, destroying vegetation and depositing material along the roadside, which reduced carriageway width and clogged drainage. Downhill at chainage 1+752 m, the slope comprising loose road-cut material with no protective measures showed significant post-monsoon damage, including erosion of almost half the road width and persistence of large gullies, indicating high vulnerability to future instability.
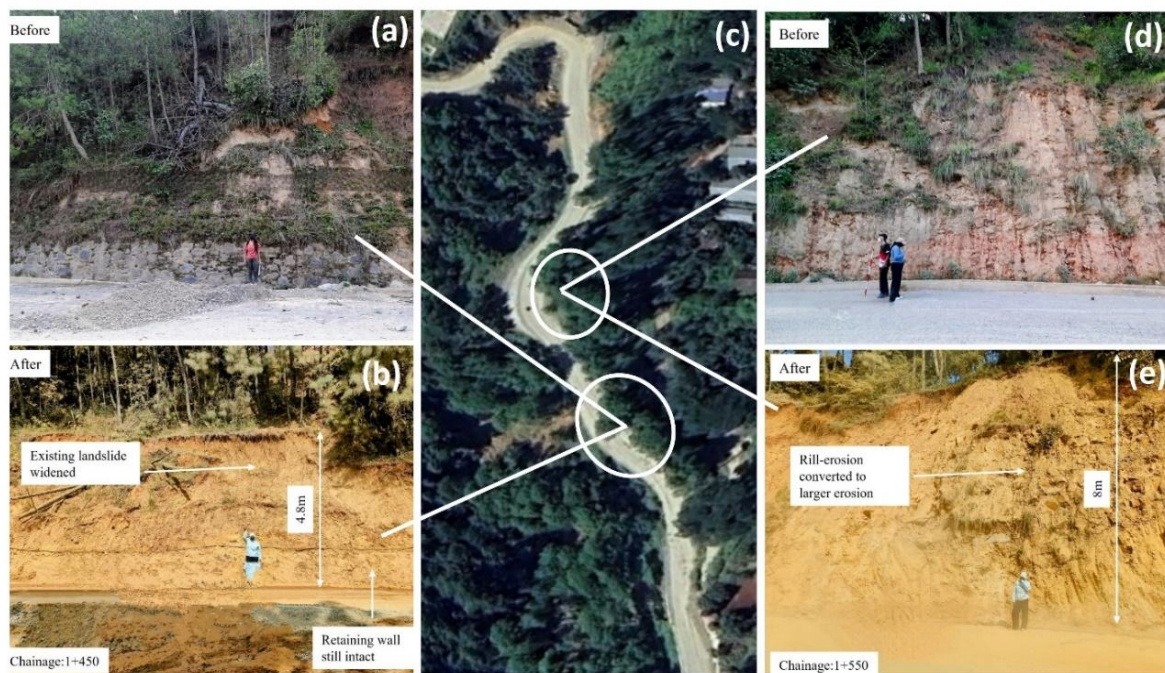
Figure 5: Pictorial comparison of before and after the monsoon at different chainage; (a) Before monsoon picture of chainage 1+450, (b) After monsoon picture of chainage 1+450, (c) Satellite Map of the alignment part, (d) Before monsoon picture of chainage 1+550, and (e) After monsoon picture of chainage 1+550

Further observations at chainages 1+777 and 1+788 m revealed that a cross-drainage structure and a natural gully, present before the monsoon, suffered badly after the monsoon as the gully widened and the drainage structure got clogged, reducing runoff discharge capacity. Unprotected soil deposited downhill was washed away, causing partial damage to an adjacent gabion wall. At chainage 2+554 m (downhill), the absence of drainage provisions led to uncontrolled water flow forming gullies up to 0.5 m deep, transporting sediment downslope and damaging agricultural fields and a secondary access road. Additionally, at chainage 2+742 m (uphill), a vertical cut slope about 4.2 m high with small pre-monsoon gullies experienced severe erosion post-monsoon, with large gullies forming along concentrated water paths and side drains clogged by soil deposits. Lastly, at chainage 4+031 m, critical river training structures, including gabion and retaining walls protecting a culvert and road boundary, were destroyed by floodwaters, leaving the culvert foundation exposed and the adjoining roadway extensively damaged, posing serious risks to transportation safety.
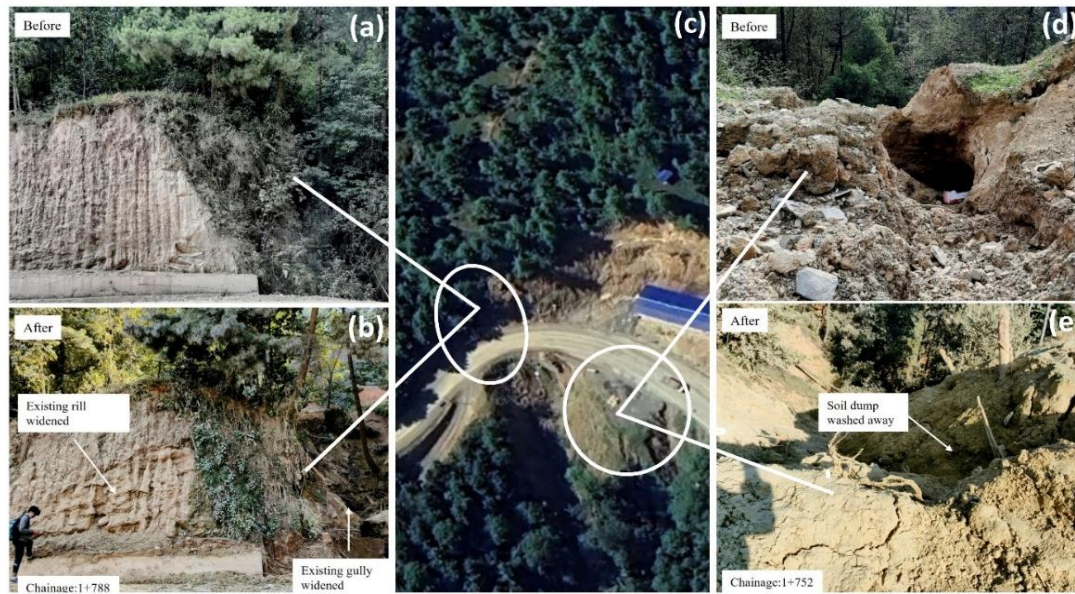

Figure 6: Pictorial comparison of before and after the monsoon at different chainage; (a) Before monsoon picture of chainage 1+788, (b) After monsoon picture of chainage 1+788, (c) Satellite Map of the alignment part, (d) Before monsoon picture of chainage 1+752, and (e)After monsoon picture of chainage 1+752
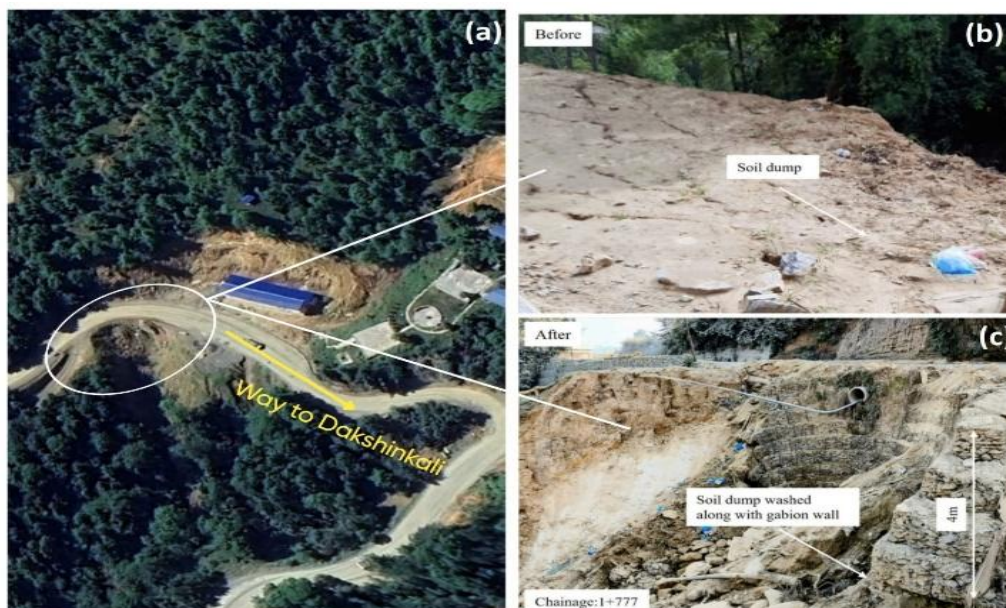

Figure 7: Pictorial comparison of before and after the monsoon at different chainage: (a) Satellite Map of the alignment part, (b) Before monsoon picture of chainage 1+777, and (c) After monsoon picture of chainage 1+777

Figure 8: Pictorial comparison of before and after the monsoon at different chainage; (a) Before monsoon picture of chainage 2+742, (b) After monsoon picture of chainage 2+742, (c) Satellite Map of the alignment part, (d) Before monsoon picture of chainage 2+554, and (e) After monsoon picture of chainage 2+554

Figure 9: Pictorial comparison of before and after the monsoon at different chainage; (a) Satellite Map of the alignment part, (b)Before monsoon picture of chainage 4+031, and (c) After monsoon picture of chainage 4+031

Figure 10: Pre- and Post-Monsoon Comparison of ECM at Failed Sections

Among the 188 chainages/sections studied, 62 sections encountered significant slope failures: 14 on uphill, 26 on downhill and 22 on both sides. Among the slope failure sections, the patterns observed were presented in the Figure 10, suggested that most of the failed sections did not have any erosion ECM. And those which did have ECM in place, the measures were insufficient to prevent slope failures and thus were badly collapsed or distorted post-monsoon.

As per the DoR recommendations (DoR-GoN, 2007), for cut heights up to 15 m, the preliminary cut slope angle for road excavation should be 40 to 63° in soft rock and 51 to 73° in hard rock. But the observed cut slope angles at failed sections were:
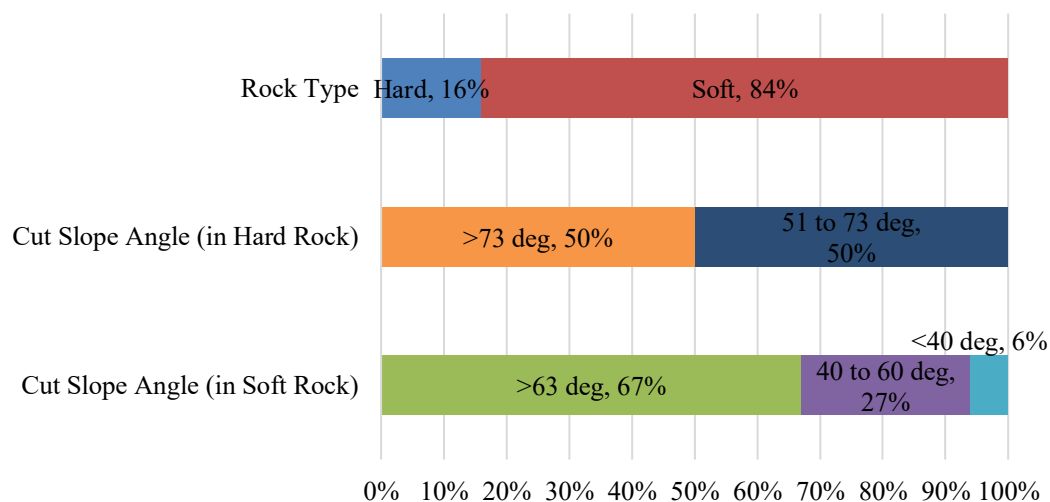

Figure 11: Rock type and Cut slope angle composition at Failed Sections

9

This shows that slope failure was more common in areas with soft rocks, and that DoR guidelines were not followed properly during road excavation – excavating roadside slopes at angles greater than that recommended by DoR- and have therefore resulted in slope failures. Moreover, some slopes were indeed cut at a slope angle equal to or less than the DoR recommended angle but still endured landslides, which may also hint towards the insufficiency of the current DoR recommendations and the need for their upgrading.
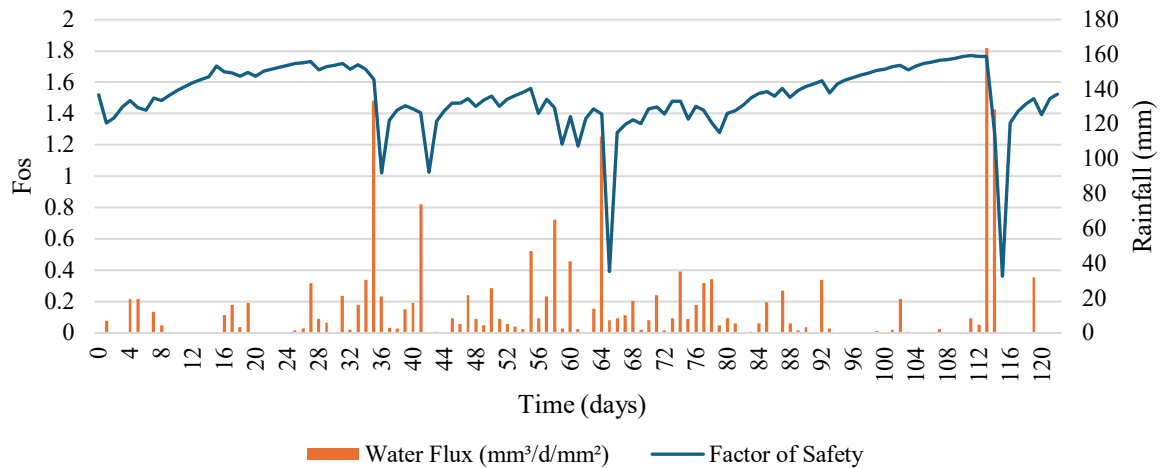
Numerical analysis

Figure 12: FOS vs Rainfall Vs Time graph for chainage 0+640m

The initial site was a sloped terrace farm uphill, with vertical cuts in the soil at certain points along the chainage and reinforced with a short retaining wall of 3m height. The initial factor of safety for the site was 1.34. Analysis suggested a plane failure, particularly at high risk on days 65 and 115, with the factor of safety dropping to as low as 0.36. Notably, the factor of safety also decreased to 1 as early as days 36 and 42. The actual site showed wedge failure with the retaining walls overtaken by debris, drains filled with soil, and the large mass movement exposed the uphill land and house to the risk of further damage. Failure is attributed to the insufficient design of the retaining wall, coupled with the geometry of the section alongside the classification of the soil on site as loamy sand, which is generally prone to waterlogging, and therefore highly sensitive to rainfall. It is possible that the initial failure originated from the section with the vertical cut, which allowed further mass movement to occur.
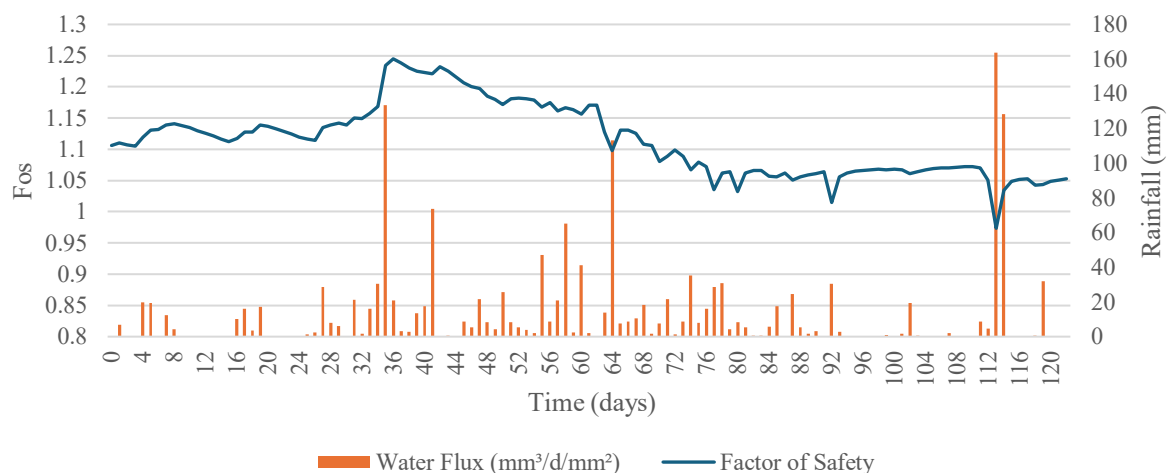

Figure 13: FOS vs Rainfall Vs Time graph for chainage 0+980m

The factor of safety (FoS) at this chainage was also greater than 1 before the monsoon. As rainfall started, FoS started to vary in reaction to the pattern of infiltration and water flux. At moderate early storms, partial saturation raised stability at some point temporarily, a phenomenon due to the increase in matric suction. But sustained infiltration decreased this stabilizing effect. The heavy rains caused pore-water pressures that continued to reduce the FoS. According to the results, limited rainfall does not instantly cause failure, which indicates that the slope could tolerate a certain level of precipitation. However, persistent and heavy rainfall quickly moves FoS downward until slope failure eventually occurs. Overall, the correlation analysis shows that the water flux due to rainfall has a strong negative dependence on slope stability. Infiltration into deeper layers of soil causes sudden decreases in FoS, and long-term seepage will not allow restoring the stability state; the slope remains in a very dangerous position. Consecutive severe storms increase the pace of this degradation process, eventually lowering FoS to life-threatening levels and slope failure.
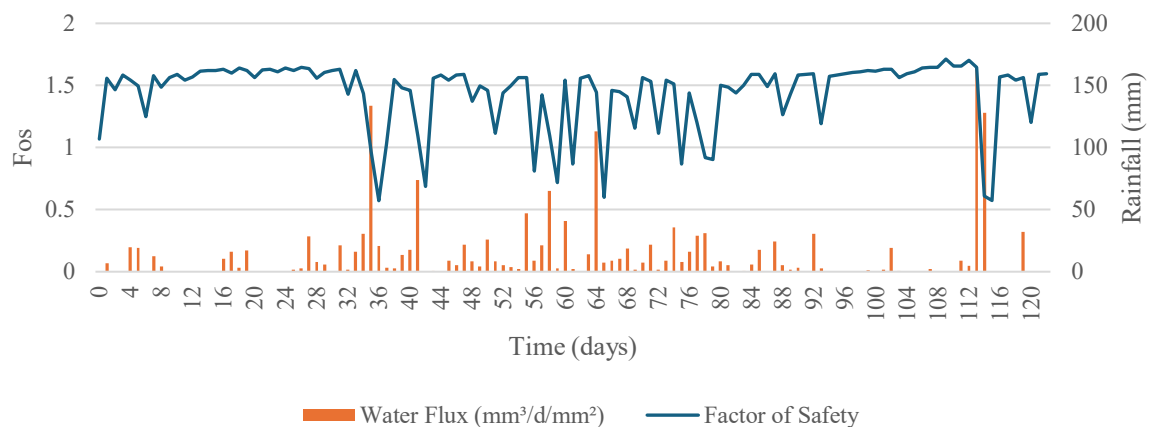

Figure 14: FOS vs Rainfall Vs Time graph for chainage 1+550m

Initially, the site had steep cuts of approximately 70 °, 10m in height uphill, with the provision of a retaining wall 4m in height. Soil from the cut slope was deposited downhill. Still, it was not relevant to the slope stability analysis as it covered the existing retaining structure, which kept the road stable. The initial factor of safety was found to be 1.06. Analysis suggested a plane failure with steep drops in factor of safety throughout the monsoon season, which shows very high sensitivity to rainfall conditions. The Factor of safety dropped to less than 1 on several instances, notably days 36, 42, 56, 59, 114, and more. The actual site showed erosion along a large span of 40m with a crown height of about 10m, which corresponds to the analysis results. Multiple large gully erosions were also observed further than 10m. The resulting erosion covered both the drainage measures and retaining walls. Failure is attributed to the heavy rainfall alongside the properties of the site soil, as the analysis suggested a high correlation with rainfall, and evidence of water erosion was clearly present during the site visit.
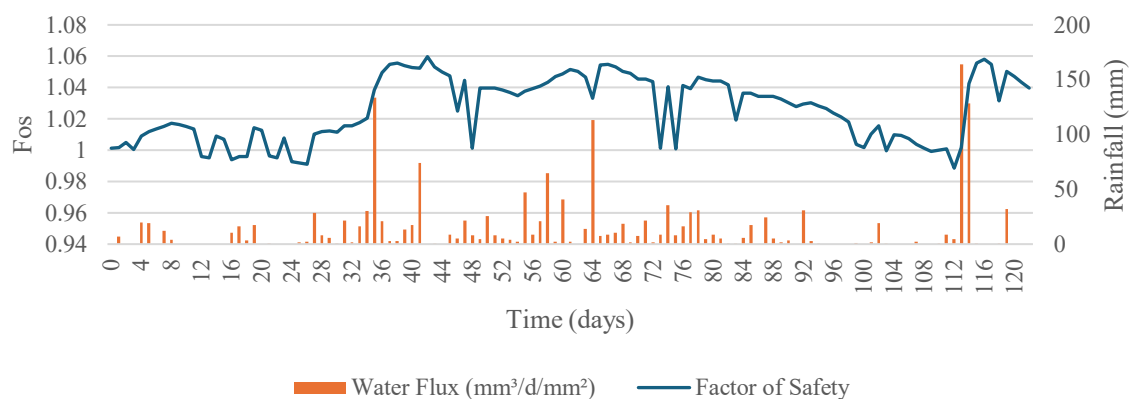

Figure 15: FOS vs Rainfall Vs Time graph for chainage 1+760m

Initially, before the onset of monsoon rainfall, the factor of safety for this chainage was satisfactory, i.e., it was above 1. As soon as the precipitation started, the factor of safety began to decrease. The factor of safety dropped enormously during intense precipitation. The graph of the factor of safety illustrates the high risk of the site as the factor of safety prominently dropped with the slightest precipitation. The analysis brought out the high peaks of infiltration during the storms and the seepage that followed, which sustained the pore-water pressure build-up and delayed the recovery of stability. These results bring attention to the extreme effect of rainfall on the slope, as it is only marginally stable and is highly impacted by aggressive storms. Overall, these results point out the likelihood of the factor of safety dropping below unity and the slope failing due to extreme rainfall events or consecutive rainfalls, in addition to bringing attention to the need for drainage and constant monitoring.
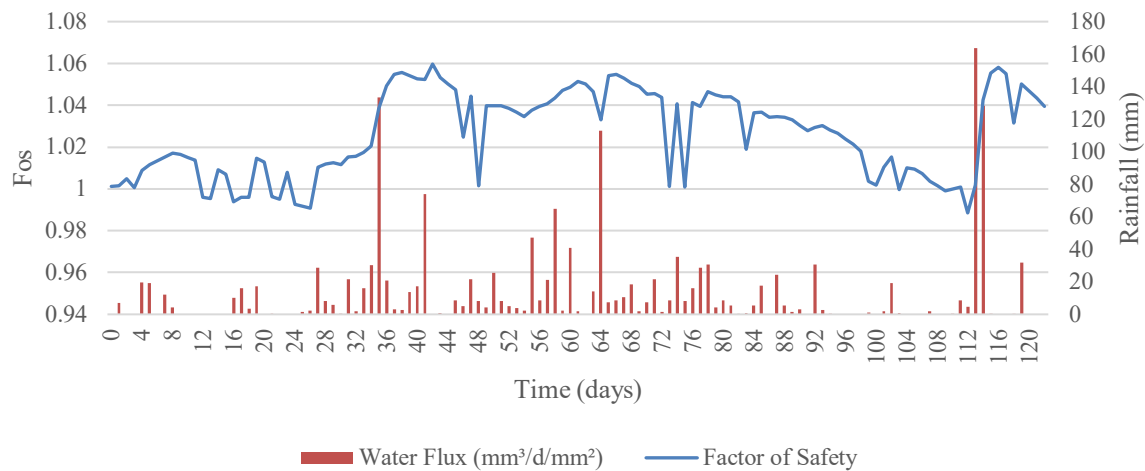

Figure 16: FOS vs Rainfall Vs Time graph for chainage 3+897

Pre-monsoon, the site was a fresh-cut soil slope of height about 7m and 70° angle with no ECMs present uphill except for the side drain. Analysis suggested a plane failure, but also that the section was initially unstable. Back analysis showed the actual properties of the slope to be much greater than the laboratory data for the slope to be initially stable, exceeding the range of values for loamy sand. Some correlation was found between the FoS and rainfall. The actual site showed large erosion on the top layer of the slope, revealing a layer of gravel underneath the soil layer. This suggested that the interlocking action of the gravel layer contributed greatly to the overall stability of the slope, and during rainfall, only the top layer of weak soil was eroded, resulting in plane failure for the soil layer only. Drains were found to be clear, likely cleaned up before the post-monsoon site visit.

Conclusion and Recommendations

The study of the Dakshinkali-Kulekhani road corridor confirms the significant impact of monsoon rainfall on roadside slope stability. A strong inverse relationship between rainfall intensity and factor of safety was observed, with repeated heavy rainfall events preventing recovery and accelerating slope failure. Specifically, four critical days (Days 35, 64, 113, and 114) recorded rainfall exceeding 100 mm/day, resulting in sharp declines in slope stability the following day. The primary cause of slope failure was identified as rainwater infiltration, which increased pore water pressure and reduced the factor of safety to critical levels. The study also revealed shortcomings in the design and implementation of erosion control measures, highlighting the urgent need for more conservative design criteria to ensure the safety of infrastructure, local residents, and travelers.

To reduce risks associated with rainfall-induced slope instability, maintaining and effectively managing side drains to ensure runoff is directed to cross-drainage structures is recommended. Prioritizing bioengineering approaches could further enhance slope resilience. Furthermore, the interaction and response of different types of soil to various rainfall intensities and durations should be considered, and to get more precise results, detailed subsoil investigations focusing on groundwater

depth and bedrock profile are recommended. It is important to note that this study covers only a short, 4 km section of the road corridor, which limits the ability to generalize findings across Nepal's diverse mountainous regions. However, similar rainfall-triggered slope failures are likely elsewhere due to comparable geological and climatic conditions, underscoring the need for site-specific investigations for improved slope protection.

References

Alias, R., Matlan, S. J., & Kasa, A. (2020). Finite element performance with different mesh sizes of retaining walls. *International Journal of Advanced Research in Engineering and Technology, 11*(4), 381–389.

Ayyub, A., Alshameri, B., Jamil, S. M., & Nawaz, M. N. (2021). Analysis of gabion retaining wall using analytical and numerical modelling with PLAXIS 2D. *UW Journal of Science and Technology, 5*.

Dahal, R. K., & Hasegawa, S. (2008). Representative rainfall thresholds for landslides in the Nepal Himalaya. *Geomorphology, 100*(3–4), 429–443. https://doi.org/10.1016/j.geomorph.2008.01.014

Dahal, R. K., Hasegawa, S., Masuda, T., & Yamanaka, M. (2006). Roadside slope failures in Nepal during torrential rainfall and their mitigation. In *Proceedings of the International Symposium on Interpraevent 2006: Disaster mitigation of debris flows, slope failures and landslides* (pp. 503–514). Japan.

Department of Roads, Government of Nepal. (2007). *Roadside geotechnical problems: A practical guide to their solution*. Kathmandu, Nepal.

Department of Roads, Government of Nepal. (n.d.). *Pavement design guidelines*.

Fredlund, D. G., & Rahardjo, H. (1993). *Soil mechanics for unsaturated soils*. John Wiley & Sons. https://doi.org/10.1002/9780470172759

van Genuchten, M. T. (1991). *The RETC code for quantifying the hydraulic functions of unsaturated soils* (EPA Report No. 600/2-91/065). U.S. Environmental Protection Agency.

GeoSlope International Ltd. (2022). *GeoStudio: SLOPE/W and SEEP/W* (Computer software). Seequent.

GeoSlope International Ltd. (2022). *Material model: Mohr–Coulomb* (Technical documentation). Seequent.

Hoek, E., & Brown, E. T. (1997). Practical estimates of rock mass strength. *International Journal of Rock Mechanics and Mining Sciences, 34*(8), 1165–1186.

Iverson, R. M. (2000). Landslide triggering by rain infiltration. *Water Resources Research, 36*(7), 1897–1910. https://doi.org/10.1029/2000WR900090

Karki, R., Hasson, S. U., Schickhoff, U., Scholten, T., & Böhner, J. (2017). Rising precipitation extremes across Nepal. *Climate, 5*(1), Article 4. https://doi.org/10.3390/cli5010004

Liu, Y., Deng, Z., Wang, X., Llorente Isidro, M., & Moncoulon, D. (2021). The effects of rainfall, soil type, and slope on rainfall-induced shallow landslides. *Applied Sciences, 11*(24), Article 11652. https://doi.org/10.3390/app112411652

McAdoo, B. G., Quak, M., Gnyawali, K. R., Adhikari, B. R., Devkota, S., Rajbhandari, P. L., & Sudmeier-Rieux, K. (2018). Roads and landslides in Nepal: How development affects environmental risk. *Natural Hazards and Earth System Sciences, 18*, 3203–3210. https://doi.org/10.5194/nhess-18-3203-2018

Ministry of Home Affairs, Government of Nepal. (2024). *A preliminary loss and damage assessment of flood and landslide: September 2024*. National Disaster Risk Reduction and Management Authority.

Paudyal, P., Dahal, P., Bhandari, P., & Dahal, B. K. (2023). Sustainable rural infrastructure: Guidelines for roadside slope excavation. *Geoenvironmental Disasters, 10*, Article 11. https://doi.org/10.1186/s40677-023-00240-x

Petley, D. N., Hearn, G. J., Hart, A., Rosser, N. J., Dunning, S. A., Oven, K., & Mitchell, W. A. (2007). Trends in landslide occurrence in Nepal. *Natural Hazards, 43*(1), 23–44. https://doi.org/10.1007/s11069-006-9100-3

Pyakurel, A., K.C., D., & Dahal, B. K. (2024). Enhancing co-seismic landslide susceptibility, building exposure, and risk analysis through machine learning. *Scientific Reports, 14*, Article 54898. https://doi.org/10.1038/s41598-024-54898-w

Schneider, S., Mallants, D., & Jacques, D. (2012). Determining hydraulic properties of concrete and mortar by inverse modelling. *Materials Research Society Symposium Proceedings, 1475*. https://doi.org/10.1557/opl.2012

Sim, K. B., Lee, M. L., & Wong, S. Y. (2022). A review of landslide acceptable risk and tolerable risk. *Geoenvironmental Disasters, 9*, Article 3. https://doi.org/10.1186/s40677-022-00205-6

Sitaula, R., Sharma, P., Chidi, C. L., & Acharya, S. (2023). Spatio-temporal analysis of landslide distribution and its impacts in Nepal. *The Geographic Base, 10*(1), 46–60. https://doi.org/10.3126/tgb.v10i01.71826

Voit, K., & Kuschel, E. (2020). Rock material recycling in tunnel engineering. *Applied Sciences, 10*(8), Article 2722. https://doi.org/10.3390/app10082722